DOI: 10.1002/adem.((please add manuscript number))
Article type: Full paper

Manufacturing of large-scale titanium-based porous transport layers for polymer electrolyte membrane electrolysis by tape casting**

By *Franz Josef Hackemüller*, *Elena Borgardt*, *Olha Panchenko*, *Martin Müller*, *Martin Bram**

[*] *Dr. Martin Bram*
Forschungszentrum Jülich GmbH, Institute of Energy and Climate Research (IEK), 52425 Jülich, Germany
m.bram@fz-juelich.de

Franz Josef Hackemüller, Dr. Elena Borgardt, Olha Panckenko, Dr. Martin Müller
Forschungszentrum Jülich GmbH, Institute of Energy and Climate Research (IEK), 52425 Jülich, Germany

[**] *This study was funded by the Federal Ministry for Economic Affairs and Energy (BMWi) as part of the NeStPEL project (funding reference no. 03ET6044A). We are very grateful for the funding received. We would also like to thank Alexander Spies from Siemens for conducting electrochemical tests in the industrial electrolyzer. Furthermore, we want to express our thanks to our second industrial partner, GKN Sinter Metals (Harald Balzer, Astrid Wierhake), for their experimental support.*

Keywords: titanium, porous, tape casting, transport layer, PEM electrolysis, electrochemical characterization

Abstract: Polymer electrolyte membrane (PEM) electrolysis is an ideal method for the direct conversion of regenerative energy into hydrogen. A key component of PEM electrolysis stacks is the porous transport layer (PTL), which is usually comprised of titanium to withstand the harsh conditions of water splitting. This present study investigates the potential of tape casting as a means of mass producing titanium transport layers in a cost-effective way. Gas-atomized and hydrogenation–dehydrogenation titanium powders were used as starting materials. A systematic study was conducted to find processing parameters, which can demonstrate the potential of tape casting as a means of manufacturing large-scale porous transport layers for PEM electrolyzers. For proof of concept, the dimensions of the porous

transport layer were scaled up to 470 x 470 mm^2 (at a thickness of 300 µm) and the component was successfully operated in an industrial electrolyzer under realistic conditions.

1. Introduction

To meet the challenges of global warming, current power sources such as fossil and nuclear fuels will need to be replaced by renewable energies.[1] Most renewable energy sources are intermittent, such as wind and solar power. To ensure a constant and stable energy supply based on renewable energy, high-performance, large-scale electrochemical energy conversion and storage devices are required. In this context, the direct conversion of electrical energy into chemically bonded energy by water splitting in an electrolyzer enables the storage of large amounts of energy, if combined with a suitable hydrogen infrastructure.[2,3] At present, water splitting based on polymer electrolyte membrane (PEM) electrolysis is one of the most promising options, since the technology is already available, free of CO_2 emissions, and proven on an industrial scale.[1,4] A detailed description of the functional principle of PEM electrolysis can be found elsewhere.[5] Due to the modular design of PEM electrolyzers, connecting single membranes in series into stacks,[6] they are of particular interest for decentralized hydrogen production, precisely adapting the size of the electrolyzer to the specific energy conversion demand. Furthermore, PEM electrolyzers enable dynamic operation and are even highly efficient if operated under partial-load conditions.[1,5,7] Nevertheless, there is a strong need to reduce the production costs of PEM electrolyzers to ensure the technology is ready for the market.

It is not just membranes, catalyst layers (CLs), and bipolar plates (BPPs) that account for the cost of PEM electrolyzer stacks, but also porous transport layers (PTLs). The layers are also known as gas diffusion layers (GDLs) or liquid/gas diffusion layers (LGDLs).[8,9] The

complex profile of PTL requirements is described in detail by numerous authors.[7-13] The PTL must enable:

- electrical contact between the CL and the BPP, which requires a low through-plane electrical resistance of the PTL bulk and a low interfacial resistance in the contact areas
- thermal conductivity for effective thermal management
- efficient gas/water transport to facilitate transport and the uniform distribution of reactants (liquid water) and products (gaseous hydrogen and oxygen) between the CL and the BPP
- mechanical stability and smooth surface topography to avoid damaging the CL and membrane during assembly and operation, especially when operating in high differential pressure mode

On the anode side, the transport layer should ideally be made of titanium to withstand the harsh operating conditions specific to water splitting. These include:[14]

- contact with water and pure oxygen at temperatures of up to 80°C
- voltages higher than the breakthrough potential of titanium.

In order to reliably prevent breakthrough corrosion on the anode side, the PTL must form a stable passivation layer, which might reduce electrochemical performance due to the higher area-specific resistance of the passivation layer compared to the blank metal.[15] To overcome this limitation, functional coatings on the PTL might be a promising alternative to keep the contact resistance low.[16]

The microstructure of the PTLs must be well designed to ensure efficient operation of the PTL in PEM electrolyzers. To achieve optimum electrochemical performance, an ideal compromise must be found in terms of thickness, mechanical stability, electrical and thermal conductivity, porosity, pore size, tortuosity, surface roughness, and surface passivation.

Furthermore, cost-effective manufacturing technologies are a prerequisite, since PTLs are one of the main cost drivers of PEM electrolyzers.

The development of PTL for PEM electrolyzers is the subject of numerous studies in literature.[7-9, 11-13, 17-24] On the anode side, three concepts are mainly used:

i.) Titanium meshes.[19, 21-23] Meshes can be produced from titanium fibers by weaving technology or by pressing with subsequent sintering. Meshes are usually characterized by larger pore diameters (e.g. around 60 µm[19]) that enhance the risk of large gas bubbles forming, which might hinder water transport.[21] Furthermore, contact resistance at interfaces is enhanced by a small amount of contact points, especially at the CL interface. The electrochemical performance of titanium meshes is therefore usually lower than that of PTL made from titanium powders or perforated titanium sheets.

ii.) *Perforated sheets.*[9,13] Thin perforated titanium sheets prepared using lithographical methods were recently introduced as a PTL for PEM electrolysis.[13] The thickness of the sheets was 25 µm and the pore diameter was adjusted in the range of 100–800 µm. Porosity was around 30 %. The PTL exhibited very promising electrochemical properties (down to 1.67 V at 2 A/cm^2). The thin perforated sheet was modified by a sprayed micro porous layer starting with µm-sized titanium particles to further improve gas transport in the PTL.[9]

iii.) PTL composed of titanium powders.[12,14,20,24] If PTLs are made from titanium powders, porosity and pore size can be easily adjusted by choosing the right powder fraction and sintering parameters. There are various ways of shaping titanium powders to porous tapes. In principle, commercial filter plates are suitable for use as PTLs. They are usually produced by pressing and sintering irregularly shaped titanium powders. For example, a commercial

titanium plate with a porosity of 30 % and an average pore diameter of 17 µm was operated in a PEM electrolyzer, achieving moderate performance.[20] In the same work, a free-standing PTL was produced by vacuum plasma spraying gas-atomized titanium powders. It was concluded that porosities > 22 % and a pore diameter in the range of 6–11 µm are optimal for achieving high electrochemical performance. Furthermore, VPS can be used to produce PTLs with a gradient in porosity by coating a thin titanium layer on a porous filter plate.[8,20] Another relatively simple yet effective approach is the free sintering of titanium powders in a powder bed. Grigoriev et al. reported optimum electrochemical performance for a PEM electrolysis cell when the porosity of the PTL was adjusted in the range of 30–50 % and the pore diameter around 12–13 µm.[12] Gas-atomized, spherical titanium powders with a particle size in the range of 50–70 µm were used to achieve such a microstructure. The thickness of the PTL was in the range of 0.8–1.4 mm. Powder rolling is a promising approach for the automated shaping of titanium powders. This process has been around since the early 1950s[25] and was recently adapted to manufacture large-scale porous titanium sheets starting with hydrogenation–dehydrogenation (HDH) titanium powders.[26] The authors demonstrated that such sheets are suitable for use as electrodes and a catalyst support for electrolysis. Another method for the fully automated manufacturing of large-scale sheets from ceramic and metal powders is tape casting. This method has been used for ceramic powders since the 1940s[27-29] and was successfully adapted to manufacture porous titanium sheets by several authors.[30-32] Compared to other methods, tape casting allows the thickness of the porous titanium sheets to be adjusted precisely in the range of 100–1000 µm and ensures high surface quality. The process is therefore particularly suited to manufacturing thin anode transport layers for PEM electrolyzers. Automated manufacturing combined with a thin layer thickness is particularly appealing from an economic standpoint, while a smooth surface improves the electrical contact with the PEM cell and protects it from mechanical damage if operated at a high differential pressure.

The present study demonstrated the potential of tape casting as a cost-effective means of manufacturing large-scale, titanium-based porous transport layers. Gas-atomized (GA) titanium powders with a spherical shape and hydrogenation–dehydrogenation (HDH) titanium powders with an angular shape were used as starting materials. From an industrial perspective, the application of HDH powders is preferable due to their lower cost compared to gas-atomized powders (factor 3–5). The tape casting slurry was adapted to the specific needs of both powders and the tape casting technology was scaled up with HDH powder to a size of 470 x 470 mm^2. Proof of concept was achieved by electrochemical testing of PTLs combined with PEM cells in a lab-scale testing device with an active cell size of 42 x 42 mm^2. The thickness was varied between 250 µm and 500 µm. The preferred processing conditions for scaling up were determined based on this study. Finally, a tape-cast PTL was operated at Siemens (Erlangen, Germany) in a large-scale laboratory electrolyzer, which was based on the SILYZER 200 concept.[33] The latter is a modular concept consisting of basis skids, each with a capacity of 1.25 MW. Another specific feature of the concept is that it can operate at a high pressure of up to 35 bar.

2. Experimental

Tape casting of titanium tapes: Two different kinds of titanium powders were used as starting materials. Gas-atomized titanium powders with a spherical shape were purchased from TLS Technik (Ti-GA, Batch 1004591, Bitterfeld, Germany). The particle size distribution of the powder was d_{10} = 18 µm, d_{50} = 28 µm, and d_{90} = 42 µm, while the tapping density (i.e. the packing density of powder particles in a container after tapping) was 2.8 g/cm^3. The interstitial content of the powder was 0.165 ± 0.001 wt.% O and 0.005 ± 0.001 wt.% C. Irregularly shaped titanium powders produced by hydrogenation–dehydrogenation (Ti-HDH) with a particle size distribution of d_{10} = 16 µm, d_{50} = 26 µm, and d_{90} = 41 µm and a tapping

density of 1.7 g/cm^3 were purchased from Shijiazhuang Runlong Filter Materials (Shijiazhuang, China). The interstitial content of this powder was 0.359 ± 0.043 wt.% O and 0.005 ± 0.001 wt.% C.

For tape casting of the powders, alcohol-based slurries were used. The slurries contained ethanol as a solvent, Mowital (Kuraray, Japan) as a binder, and a combination of Solusolv (Solutia Inc., USA) and PEG 400 (Merck, Germany) as plasticizing agents. Due to its lower tapping density, the application of Ti-HDH powder required a higher solvent content to achieve a slurry capable of flowing. Nevertheless, the solvent content was kept as low as possible. It was adjusted in such a way that no excess solvent was left in sedimentation tests. As a second step, the binder content was optimized. Here, a binder/solvent ratio of around 0.08 was found to be the best compromise to prevent segregations in the slurry and to optimize degassing and tape casting behavior. Finally, plasticizing agents were added to ensure sufficient plasticity for the tape in the green state. **Table 1** shows the optimized composition of the slurries, adapted to the two kinds of powders used in the present study.

Table 1: *Optimized composition of tape casting slurries adapted to Ti-GA and Ti-HDH powders. All contents are given in wt. %.*

	Slurry with Ti-GA powder	Slurry with Ti-HDH powder
Powder content	83.8	69.2
Solvent content (ethanol)	14.2	27.8
Content of binder and plasticizing agents	2.0	3.0

As expected, varying the slurry composition had a significant influence on viscosity and tape casting behavior. **Figure 1a** compares the viscosity of both slurries as a function of the shear rate. The slurry composed of Ti-HDH powders had a significantly lower viscosity due its higher solvent content. At a shear rate of 10 s^{-1}, the viscosity was 5.7 ± 0.2 Pa·s compared to a shear rate of 32.0 ± 2.0 Pa·s for the slurry based on Ti-GA powder. Nevertheless, both slurries

offered sufficient stability to reliably prevent segregation during the tape casting process and also to enable continuous casting of flawless and viscoelastic green tapes. Since the quality and handling of tapes from both powders were satisfactory, no further changes to the slurry compositions were required to scale up the technology, as described later.

The general optimization of tape casting was performed on a lab-scale tape casting device (Netzsch, Germany). An automated tape casting device (FGA500, SAMA, Germany) was used to scale up the technology. The thickness of the green tapes was systematically varied between 200 µm and 800 µm by adjusting the position of the doctor blade while maintaining a constant casting speed at 250 mm/min. **Figure 1b** shows the relationship between the position of the doctor blade, in relation to the carrier tape, and the resulting thickness of the green tapes after drying. The width of the green tapes was incrementally increased from 160 mm to 500 mm – the maximum width accessible with the FGA500 device. Green tapes were subsequently cut into rectangular pieces (140 x 140 mm^2 and 470 x 470 mm^2) using a cutting device, followed by debinding and sintering.

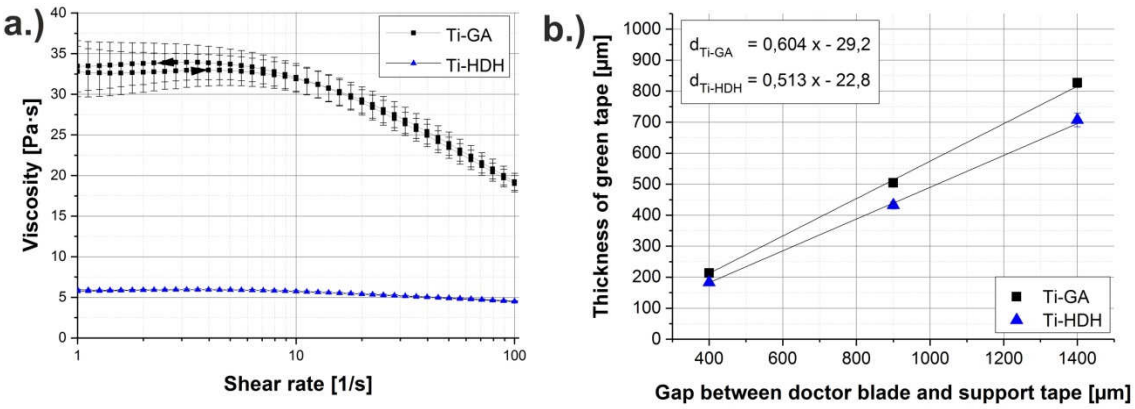

Figure 1: a.) *Viscosity of slurries comprised of Ti-GA and Ti-HDH powders.* ***b.)*** *Thickness of the green tape after drying as a function of the position of the doctor blade.*

Debinding and sintering was performed in a vacuum furnace (Thermal Technology 12-12-12-

WM, Santa Rosa, USA). The binder, plasticizer, and residual solvent were removed under flowing Ar, maintaining an average pressure of 15 mbar in the furnace chamber. Samples were thus heated at 2 K/min to 500 °C, followed by a dwell time of 30 min. Heating was then kept at 2 K/min and sintering was performed in a vacuum (10^{-5} mbar) at 800 °C, 900 °C, 1000 °C, and 1200 °C. The dwell time was 2 h for each sintering temperature. The average porosity of the tapes after sintering was calculated by geometrical mean, using a theoretical density of 4.5 g/cm^3 for titanium.

Microstructural investigation: For microstructural investigation, the porous tapes were embedded in resin and cross sections of the tapes were prepared using metallographic methods. A scanning electron microscope (TM3000, Hitachi, Japan) was used to compare the different microstructures.

Air permeability: A measuring device was built in-house to determine gas permeability. In this device, the porous transport layers were mounted between two cylindrical, acrylic glass containers. Air was fed to the bottom container and the build-up pressure was measured. Mass flow controllers were used to record the transported air volume over time.

Pore size distribution: Mercury porosimetry (Fisons Instruments, Pascal 140/Pascal 440) was used to investigate the pore size distribution of the surface of the PTLs.

Chemical analysis: Uptake of interstitial elements after sintering was investigated by chemical analysis. The oxygen level was determined by hot extraction in helium flow with subsequent thermal conductivity measurement for nitrogen and IR spectroscopy for oxygen, with a LECO TCH 600 device (LECO, Saint Joseph, USA). The carbon content of the sample

was determined by IR spectroscopy using a LECO CS 600 device (LECO, Saint Joseph, USA). The error of all measurements was < 1 %.

Mechanical tests: In order to characterize mechanical properties, tensile tests were performed on a device from Zwick GmbH & Co. KG (Allroundline ZE005 TE). The testing conditions fulfilled the requirements of the ISO 7500-1 standard. The samples were dog-bone shaped and had a thickness of approximately 1 mm. A schematic of the sample geometry is shown in **Figure S1**. Samples with lower thicknesses were found to be unsuitable for tensile testing due to premature failure. All tensile tests were performed with a preload of 5 N and a constant strain rate of 50 N/min. At least three measurements were performed for each parameter set, thus forming the basis to calculate the mean value and standard deviation.

Electrochemical characterization: The general setup of an electrochemical testing cell is shown in **Figure S2**. To investigate the influence of the thickness and porosity of the PTL on the electrochemical performance of PEM electrolysis cells, PTLs with thicknesses of approximately 250 µm and 500 µm after sintering were laser-cut to a size of 42 x 42 mm^2. The PTLs were mounted on the anode side. On the cathode side, carbon tape was used as a transport layer. A 177.8-µm-thick Nafion membrane (E300 with Nafion 117, Greenerity GmbH, Germany) was used as an electrolyte. The electrolyte was coated on the anode side with IrO_2 (Alfa Aesar) and on the cathode side with Pt (Johnson Matthey, HISPEC 9100). Current density–voltage curves were measured in galvanostatic mode with steps of 0.2 A/cm^2 and a dwell time of 5 min for each measuring point. The maximum voltage was 2.2 V. The water volume flow rate on both sides was 25 ml/min and the operating temperature of the cell was set to 80 °C.

For proof of concept, a large-scale Ti PTL was tested by Siemens (Erlangen, Germany) in a laboratory setup, which was based on the SILYZER 200 concept.[33] The active size of the PTL was 1400 cm^2 and its thickness was 300 µm.

3. Results and discussion

Figure 2a shows the tape in the green state after the casting process in the large tape casting device (F500). **Figures 2b** and **2c** show the related microstructures of tapes comprised of Ti-GA and Ti-HDH after the drying step. The binder appears in gray color partly covering the powder particles. The thickness profiles of the tapes in the green state were recorded using a micrometer caliper to estimate the homogeneity of the tape casting process. In **Figure 3**, the thickness profiles of the tapes, which were prepared starting with Ti-GA powder, are given. As expected, larger deviations occurred if the tape was cast on the lab-scale tape casting device (**Figure 3a**). These deviations are mainly caused by the slurry being filled in the device by hand. Under these conditions, it is difficult to maintain a constant filling height and hydrostatic pressure for the slurry in the device. There was significantly less deviation when the tape was cast using the automated F500 tape casting device (**Figure 3b**). In this study, the device was equipped with a tap to keep the filling height constant. In general, thickness was found to be enhanced in the middle of the tape, which is, in part, caused by the surface tension of the cast slurry. A relatively similar thickness profile was achieved with the slurry comprised of Ti-HDH powder (not shown here).

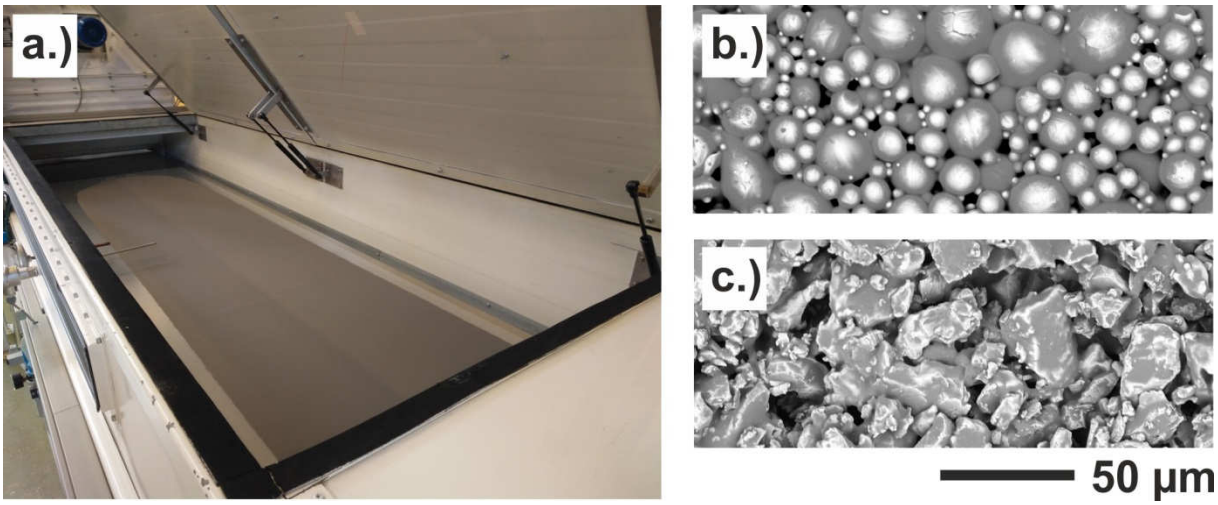

Figure 2: a.) *Green tape in the F500 tape casting device;* ***b.)*** *microstructure of the green tape produced from Ti-HDH powder;* ***c.)*** *microstructure of the green tape produced from Ti-GA powder.*

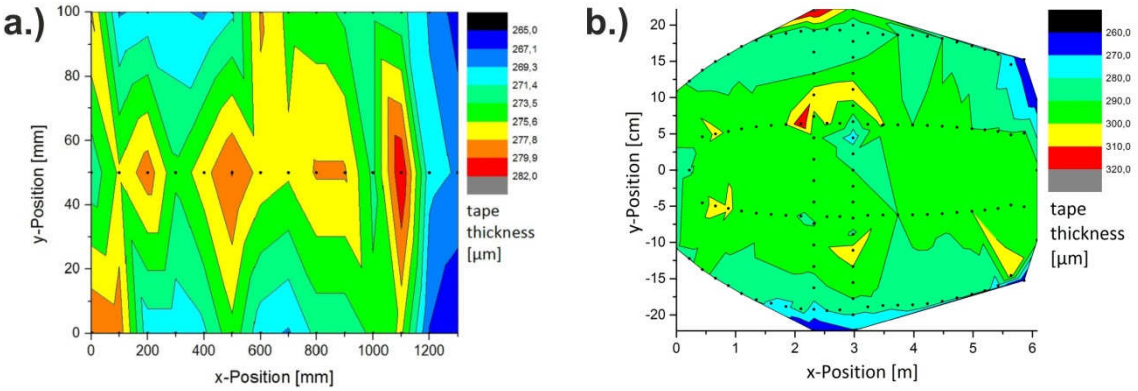

Figure3: *Thickness profiles of Ti tapes produced from Ti-GA powder* ***a.)*** *on a lab-scale tape casting device and* ***b.)*** *on an automated F500 tape casting device.*

The green tapes were subsequently assembled, debinded, and sintered at different temperatures and then laser-cut to their final dimensions. **Table 2** gives a summary of the average thickness and average porosity of all transport layers considered in this study. The samples were used to find the best combination in terms of thickness and porosity. The thickness of the sintered tapes was again measured using a micrometer caliper; porosity was measured by the geometric mean. The scattering of thickness was caused by the tape casting process, as discussed previously. In general, thickness decreased with increasing sintering

temperature due to enhanced shrinkage. As expected, tapes comprised of Ti-HDH powder exhibited – at a given sintering temperature – significantly higher porosity than those comprised of Ti-GA powder. This effect was caused by the lower tapping density of Ti-HDH powder and the lower solid content of the tape casting slurry. It was likely aggravated further by the lower sintering activity of the Ti-HDH powder due to its higher content of interstitial elements, such as oxygen and carbon. Furthermore, residual porosity was reduced with increasing tape thickness, which was likely caused by the self-weight of powder particles. This effect can be almost disregarded up to a sintering temperature of 1000 °C. Finally, the porosity of the tapes could be well adjusted in the range of 10–33 % for tapes comprised of Ti-GA powders and in the range of 15–53 % for tapes comprised of Ti-HDH powders.

Table 2: *Thickness and porosity of the porous titanium tapes used as PTLs and transport layers to test electrochemical performance with PEM electrolysis cells. The size of the transport layers was 42 x 42 mm^2 in all cases (achieved by laser cutting).*

Name	Sintering temperature [°C]	Sample thickness [µm]	Porosity [%]
Ti-GA-800-250	800	258 ± 5	32.9 ± 2.0
Ti-GA-900-250	900	263 ± 2	28.6 ± 1.4
Ti-GA-1000-250	1000	251 ± 7	19.0 ± 3.2
Ti-GA-1200-250	1200	250 ± 10	12.8 ± 4.5
Ti-GA-800-500	800	530 ± 21	31.2 ± 3.3
Ti-GA-900-500	900	494 ± 7	25.0 ± 1.8
Ti-GA-1000-500	1000	500 ± 21	15.8 ± 4.3
Ti-GA-1200-500	1200	476 ± 6	9.6 ± 2.0
Ti-HDH-800-250	800	275 ± 9	53.5 ± 2.1
Ti-HDH-900-250	900	275 ± 4	49.4 ± 1.3
Ti-HDH-1000-250	1000	244 ± 5	31.3 ± 2.3
Ti-HDH-1200-250	1200	236 ± 5	17.6 ± 2.9
Ti-HDH-800-500	800	517 ± 1	53.0 ± 0.6
Ti-HDH-900-500	900	480 ± 13	43.7 ± 2.0
Ti-HDH-1000-500	1000	455 ± 10	29.9 ± 2.3
Ti-HDH-1200-500	1200	425 ± 4	14.7 ± 1.8

Figure 4 shows the microstructures of the porous tapes, which are dependent on the sintering temperature for a sample thickness of approximately 250 µm. At temperatures above 900 °C, open porosity started to become partly closed. At 1200 °C, almost all residual pores were closed, which is critical with respect to water and gas transport in the transport layer. Furthermore, the samples tend to become distorted on a macroscopic scale due to the onset of inhomogeneous shrinkage at higher temperatures.

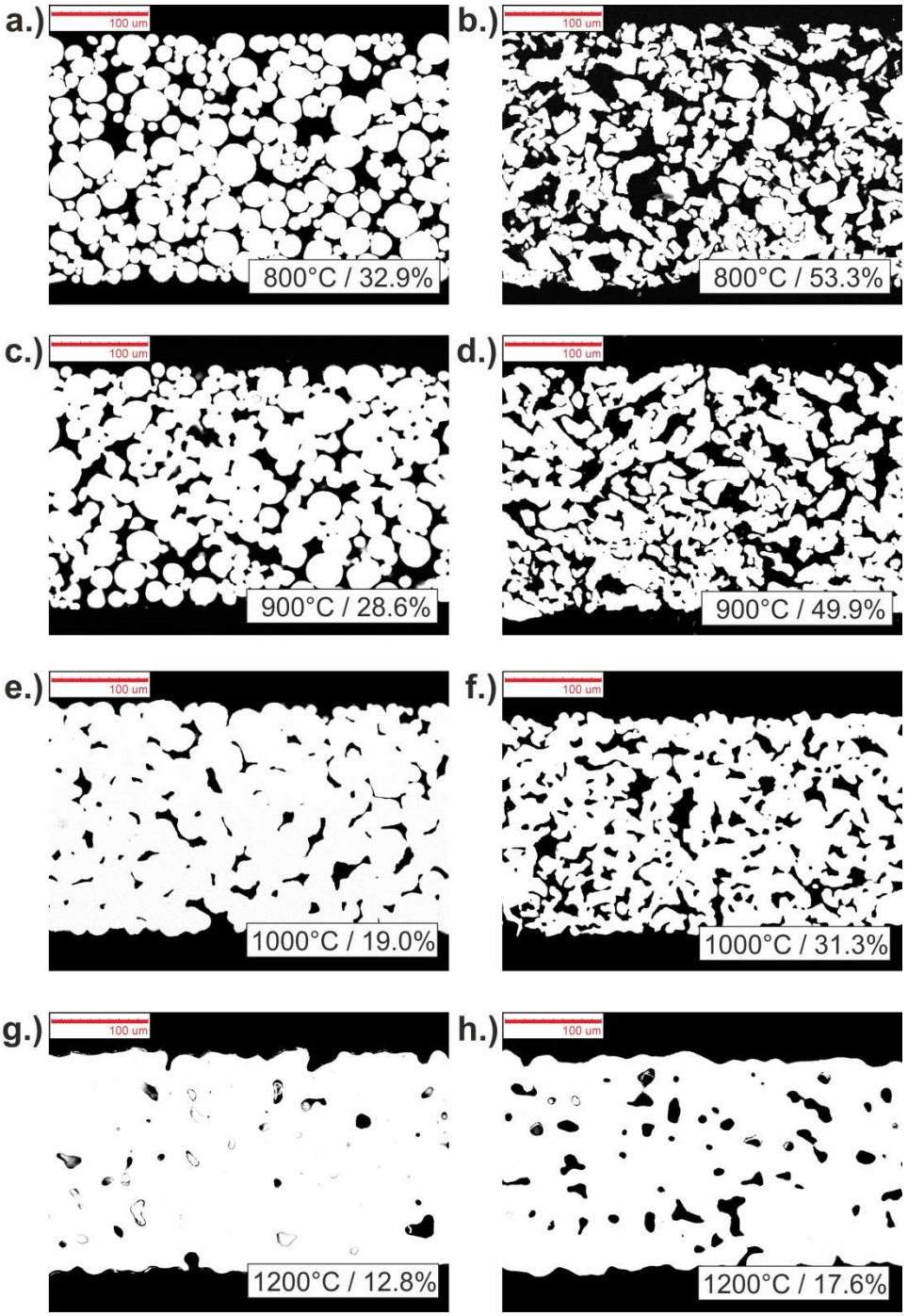

Figure 4: *Microstructures of porous titanium tapes comprised of Ti-GA powders (left-hand side) and Ti-HDH powders (right-hand side), which are dependent on the sintering temperature.* ***a.,b.)*** *Ti-GA-800-250, Ti-HDH-800-250;* ***c.,d.)*** *Ti-GA-900-250, Ti-HDH-900-250;* ***e.,f.)*** *Ti-GA-1000-250, Ti-HDH-1000-250;* ***g.,h.)*** *Ti-GA-1200-250, Ti-HDH-1200-250.*

Air permeability was measured under ambient conditions to estimate the flow resistance of the transport layers, which is dependent on the process parameters. **Figure 5a** provides a summary of the results. In the present study, a near-linear relationship was found between gas

flow and pressure drop. Permeability could thus be calculated by Darcy's law [34] at flow rates of up to 200 ml/min. The influence of turbulent flow can be almost disregarded under these conditions. The air permeability of the porous transport layers lies between $8 \cdot 10^{-13}$ m^2 and $7 \cdot 10^{-12}$ m^2, which is in good agreement with related investigations performed by Grigoriev et al. and Bromberger et al.[12,35] As an alternative to sintered tapes, porous carbon tapes with porosities in the range of 60–80 % can be used as PTLs.[36-38] Gostick et al. report maximum gas permeabilities for pure carbon tapes of up to $1 \cdot 10^{-11}$ m^2, which can be explained by their higher porosity. Nevertheless, other authors achieved permeabilities between $2 \cdot 10^{-13}$ m^2 and $9 \cdot 10^{-13}$ m^2. In this study, the carbon paper was modified by functional coatings, for example, which might explain the lower values. In terms of gas permeability, sintered porous titanium tapes are promising candidates for keeping the gas diffusion limitation of the PTL at acceptable low levels.

Another characteristic property of the PTL is the mean pore diameter. **Figure 5b** shows the mean pore radius of the sintered tapes, which is measured by mercury porosimetry. For all types of tapes, the relationship between pore radius and porosity is almost linear and the values are in the range of 3 µm to 6 µm. By trend, the pore radius was slightly larger in the case of Ti-GA powders (at a given porosity around 30 %). Grigoriev et al.[12] reported that the ideal pore radius is around 5.0–6.5 µm. In the present study, this value could only be achieved with Ti-HDH powder at a low sintering temperature (Ti-HDH-800-250). Unfortunately, mechanical stability of the tapes manufactured under these process conditions is insufficient for scaling up of the technology.

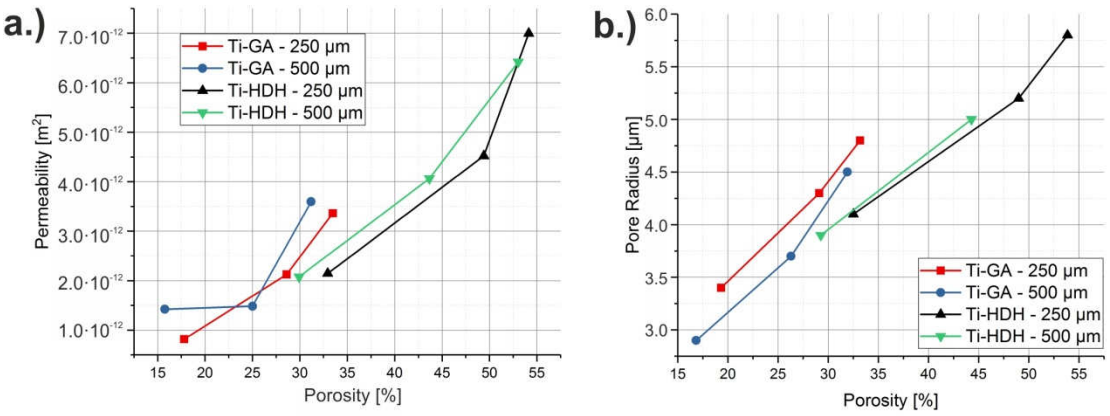

Figure 5: a.) *Air permeability of porous titanium tapes comprised of Ti-GA powders and Ti-HDH powders as a function of porosity. Measurements were performed under ambient conditions at room temperature.* ***b.)*** *Mean pore radius of porous titanium tapes measured by mercury porosimetry.*

As expected, tensile tests on titanium PTL deomonstrated the strong influence of porosity on stress–strain behavior (related curves not shown here). In the case of Ti-GA powder, an almost linear elastic behavior was observed until fracture, if the porosity value exceeded 20 %. At lower porosities, the onset of plastic deformation was also observed. In contrast, samples comprised of Ti-HDH powder clearly showed reduced plastic deformation, even at lower porosities. Nevertheless, higher fracture strengths were observed at a given porosity. In **Figure 6**, the fracture strength σ is given as a function of porosity P (in %). For both powders, a near-linear relationship was observed, which could be described by the following equations:

$$\sigma_{\text{Ti-GA}} = 511.16 - 14.07 \cdot P \text{ [MPa]} \quad (1)$$

$$\sigma_{\text{Ti-HDH}} = 657.54 - 12.63 \cdot P \text{ [MPa]} \quad (2)$$

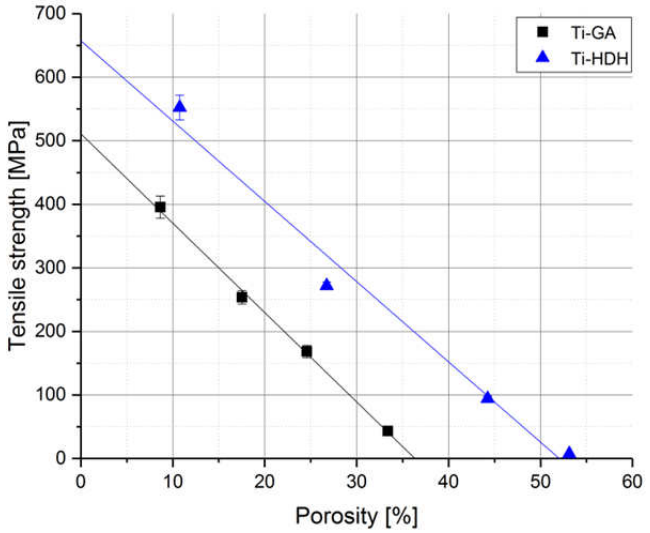

Figure 6: *Tensile strength of the porous titanium tapes as a function of porosity. The thickness of the dog-bone shaped sample was 1mm.*

Such a relationship was expected for porous titanium based on the literature.[39,40] The equations are reasonable since for P = 0 %, the calculated tensile strength approaches the respective values of bulk titanium grade 2 (485 MPa according to ISO 5832-2) for Ti-GA powder and titanium grade 4 (685 MPa according to ISO 5832-2) for Ti-HDH powder. This can be largely explained by the higher content of interstitial elements such as oxygen and carbon after sintering.[41,42] Chemical analysis of the tensile samples sintered at 1200 °C revealed an interstitial content of up to 0.500 ± 0.030 wt. % oxygen and up to 0.240 ± 0.020 wt. % carbon for Ti-GA samples. For Ti-HDH, higher values of up to 0.740 ± 0.080 wt. % oxygen and up to 0.254 ± 0.012 wt. % carbon were found. In general, the scattering of interstitial content was observed after different sintering runs. The maximum values are therefore reported here. The failure of the samples might also be influenced by the angular pore shape, which acts as a notch for crack initiation and is more pronounced in Ti-HDH powder. A more detailed study on the mechanical properties of porous titanium transport layers was recently published.[37] In this study, the mechanical strength of the transport layers was investigated under more realistic conditions. A specific experimental setup allowed the

mechanical response of the transport layers to be estimated for PEM cells operated with high pressure differences of up to 50 bar.

Finally, electrochemical characterization of PEM electrolysis cells was performed for all types of transport layers, as defined in **Table 2**. **Figure 7** provides a summary of the results for all related current density–voltage curves. At low current densities, the deviation from linearity is mainly caused by polarization losses at the electrodes. With increasing current density, the increasing slope of the curves and the deviation from linearity to higher voltages are clear indications of mass transport limitations in the titanium-based porous transport layers.[43]

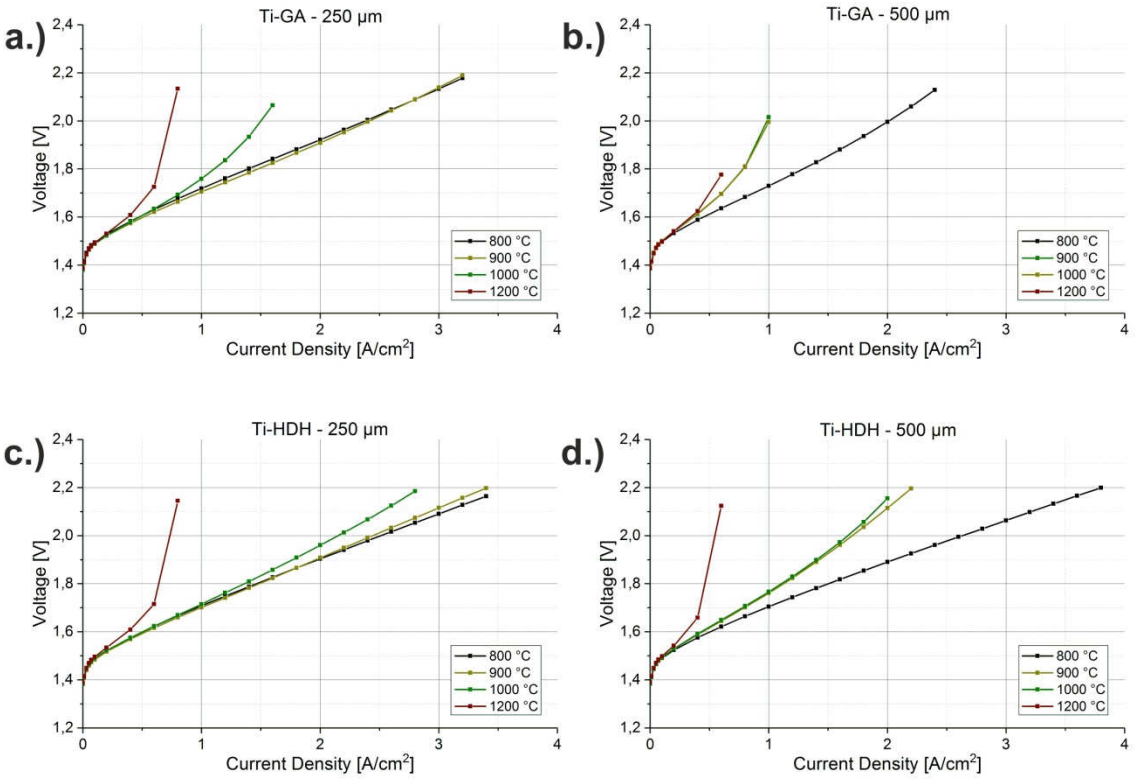

Figure 7: *Current density–voltage curves of PEM electrolysis cells measured at 80 °C with a titanium-based porous transport layer on the anode side.* ***a.)*** *Ti-GA powder, tape thickness of around 250 µm (Ti-GA-800-250 – Ti-GA-1200-250);* ***b.)*** *Ti-GA powder, tape thickness of around 500 µm (Ti-GA-800-500 – Ti-GA-1200-500);* ***c.)*** *Ti-HDH powder, tape thickness of around 250 µm (Ti-HDH-800-250 – Ti-HDH-1200-250);* ***d.)*** *Ti-HDH powder, tape thickness of around 500 µm (Ti-HDH-800-500 – Ti-HDH-1200-500).*

In the present study, best electrochemical performance was achieved with PTLs, which were manufactured at low sintering temperatures (800 °C and 900 °C). At these conditions, sintering necks were less pronounced (**Figure 4a – 4d**). This result indicates that through-plane resistance might be almost neglected if comparing the electrochemical performance of the present samples. Furthermore, it is supposed that the interface resistance to the CL also does not play a major role since there are a lot of contact points due to the small particle size of the starting powders (< 45 µm) and the smooth surface of the sintered tapes. Therefore, mass transport limitations are expected to be the main reason for differences of electrochemical performance. Nevertheless, additional impedance measurements are required to confirm this assumption.

In general, electrochemical performance of electrolysis cells operated with tape casted PTLs was in the same range compared to related studies in literature. Grigoriev et al.[12] achieved a voltage of 1.87 V at 2 A/cm^2 with a PTL produced by the free sintering of gas-atomized titanium powders (particle fraction 75–100 µm) in a powder bed. The sample had a thickness of 1.4 mm, a porosity of 40 %, a mean pore radius of 6.0 µm, and a gas permeability of $6.2 \cdot 10^{-12}$ m^2. In this work, no clear indication of mass flow limitation was found. Lettenmeier et al.[20] reported a voltage of approximately 1.95 V at 2 A/cm^2 for a commercial, 1-mm-thick porous Ti plate, which was comprised of irregularly shaped titanium particles with a particle size in the range of 100–200 µm. The plate had an average pore size of 17 µm. Electrochemical performance was improved to 1.9 V at 2 A/cm^2 when the coarse porous Ti plate was coated with a thin vacuum-plasma-sprayed titanium layer (porosity 10–15 %, pore size 1.6–3.7 µm). The improvement was mainly being attributed to the lower interfacial resistance to the CL. The authors stated that the gradient in porosity is of benefit for cell operation. Small pores near to the CL enable improved water management at high oxygen

production rates, while larger pores in the direction of the flow field moderate the rapid release of oxygen bubbles.

Compared to the literature, electrochemical performance of cells with PTLs made by tape casting from Ti-HDH and sintered at 800°C fit quite well to the results of Grigoriev et al.[12] With respect to the porosity of 47–52 %, the pore radius in the range of 4.0–6.0 µm and the permeability of $7.0 \cdot 10^{-12}$ m^2, cell voltage of approximately 1.9 V at 2 A/cm^2 is quite reasonable. Nevertheless, mechanical stability of tapes sintered at this condition is not sufficient for reliable scaling up of technology. Slightly reduced electrochemical performance was achieved with PTLs made from Ti-GA powders, which were sintered at 800°C and 900°C. Here, lower porosity in the range of 27–32 %, lower pore radius in the range of 3.5–4.5 µm and lower permeability of $3.2 \cdot 10^{-12}$ m^2 might cause the performance decrease. With increasing sintering temperature and with increasing thickness of the tape onset of mass transport limitation became obvious leading to the conclusion that there is still room for further microstructure optimization of tape casted PTLs. Possible options of improvement are the use of coarser starting powders with narrow particle size distribution, application of pore formers or introduction of vertical holes e.g. by laser treatment. Furthermore, a gradient in porosity, which can be for example easily realized by laminating tapes made from powders with different particle fractions would be another promising way of achieving further improvement.

As mentioned previously, Ti-HDH powders were preferred for scaling up from an industrial perspective due to economic reasons. To take precautions in terms of mechanical stability, the tape thickness was increased slightly to 300 µm and an intermediate sintering temperature of 1000 °C was chosen.

4. Scaling up technology

Finally, the scale-up of technology was investigated with the aim of testing titanium PTLs in an industrial-scale electrolyzer at Siemens (Erlangen, Germany). In order to adapt our technology to this device, a PTL size of 1400 cm^2 was required. In a first step, tape casting was performed starting with Ti-HDH powders and using the maximum usable width for the automated F500 tape casting device. The thickness profile of the tape was shown in **Figure 3b**. A titanium tape with a size of 470 x 470 mm^2 was subsequently assembled and sintered at 1000 °C for 2 h in a vacuum. The shrinkage of the tape was around 15 %. The average thickness of the sintered tape was in the range of 300 µm with a thickness deviation of less than 30 µm. The final dimensions of the PTL were achieved by laser cutting. **Figure 8** shows the large-scale PTL in the as-sintered state, demonstrating that it could be easily handled after sintering enabling the assembling in the electrolyzer stack. In **Figure 9**, the electrochemical performance of a PEM cell with a novel tape-cast PTL is compared to the performance of that of a Siemens laboratory setup as a reference. With respect to the reference, only slight improvement was achieved by implementing the new PTL. It became apparent that further optimization of the microstructure, process conditions, and integration in the stack is required to take full advantage of tape-cast PTLs. Nevertheless, this kind of PTL has the potential to improve contact with the PEM electrode due to its surface being smoother than established transport layers.[6,8,14,21] If PEM cells are operated at a higher pressure (the SILYZER 200 concept enables a pressure of up to 35 bar), a smooth and homogeneous interface between the transport layer and the PEM cell is expected to offer the sensitive polymer electrolyte greater protection from mechanical damage.

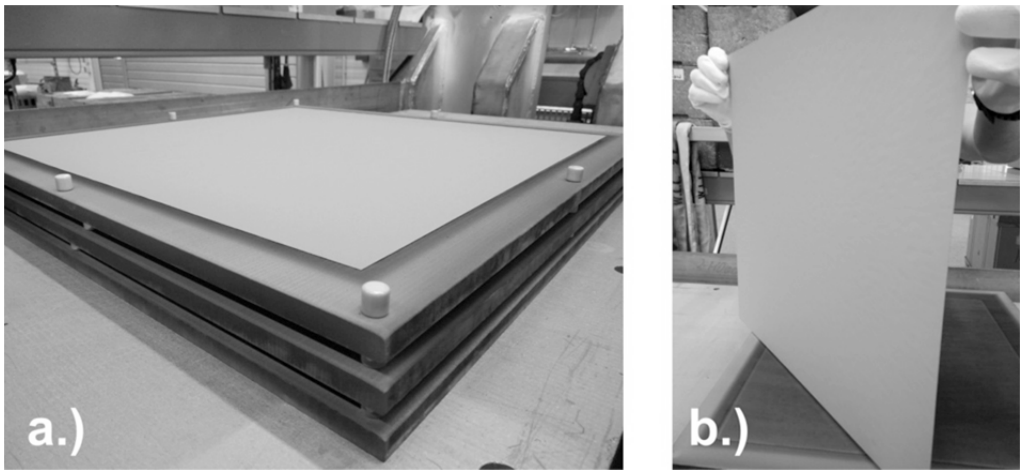

Figure 8: a.) *Porous transport layer produced by tape casting of Ti-HDH powders. Size in the green state was 470 x 470 mm^2. Sintering was performed at 1000 °C for 2 h in a vacuum.* ***b.)*** *Handling the tapes after sintering.*

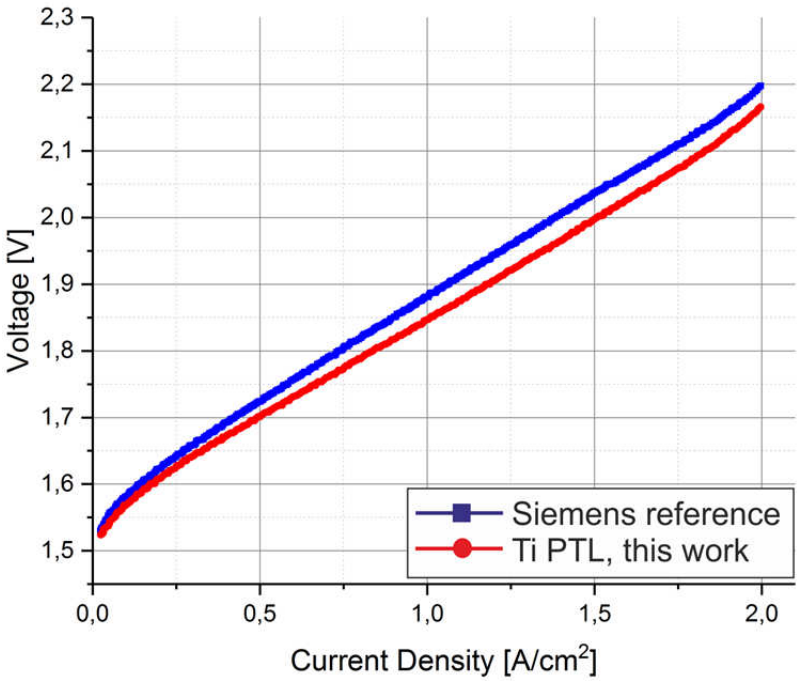

Figure 9: *Current density–voltage curve of large PEM cells operated in an industrial electrolyzer. Both configurations were operated in one stack under the same conditions. Comparison of the reference transport layer (blue color) with the novel titanium-based porous transport layer (size 1400 cm²).*

5. Conclusions

Titanium-based porous transport layers for PEM electrolysis cells were produced by tape casting with a thickness in the range of 250–500 µm and porosities in the range of 8–53 %. Gas-atomized titanium particles with a spherical shape and hydrogenation–dehydrogenation (HDH) titanium particles with an angular shape were used as starting materials. In both cases, the particle size was below 45 µm. Electrochemical testing demonstrated that this new kind of transport layer is suitable to support and establish electrical contact with the PEM electrolysis cell. The best compromise in terms of cost-effective manufacturing, mechanical stability, and electrochemical performance was achieved using Ti-HDH powder sintered at 1000 °C for 2 h in a vacuum. Under these conditions, the porosity of the transport layers was around 30 %. Using these process parameters, the technology was successfully scaled up to dimensions of 470 x 470 mm^2 (at a thickness of 300 µm) and the transport layer function was proven while taking industrial aspects into account.

Acknowledgements

This study was funded by the Federal Ministry for Economic Affairs and Energy (BMWi) as part of the NeStPEL project (funding reference no. 03ET6044A). We are very grateful for the funding received. We would also like to thank Alexander Spies from Siemens for conducting electrochemical tests in the industrial electrolyzer. Furthermore, we want to express our gratitude to our second industrial partner, GKN Sinter Metals (Harald Balzer, Astrid Wierhake), for their experimental support.

Conflicts of interests

The authors declare that they have no conflicts of interests.

Received: ((will be filled in by the editorial staff))
Revised: ((will be filled in by the editorial staff))
Published online: ((will be filled in by the editorial staff))

References

[1] H. Wendt, G.H. Vogel, *Chem. Ing. Techn.* **2014**, *86*, 144-148.

[2] B. Paul, J. Andrews, *Int. J. Hydrogen Energy* **2008**, *33*, 490–498.

[3] R.E. Clarke, S. Giddey, F.T. Ciacchi, S.P.S. Badwal, B. Paul, J. Andrews, *Int. J. Hydrogen Energy* **2009**, *34*, 2531-2542.

[4] N. Briguglio, V. Antonucci, in *PEM Electrolysis for Hydrogen Production: Principles and Applications*, (Eds. Bessarabov D, Wang H, Li H, Zhao N) CRC Press, Boca Raton, Florida, USA **2015**, 1-9.

[5] T. Smolinka, E. Ojong, T. Lickert, in *PEM Electrolysis for Hydrogen Production: Principles and Applications*, (Eds. Bessarabov D, Wang H, Li H, Zhao N) CRC Press, Boca Raton, Florida, USA **2015**, 11-33.

[6] P. Millet, R. Ngameni, S.A. Grigoriev, N. Mbemba, F. Brisset, A. Ranjbari, C. Etiévant, *Int. J. Hydrogen Energy* **2010**, *35*, 5043-5052.

[7] M. Carmo, D.L. Fritz, J. Mergel, D. Stolten D, *Int. J. Hydrogen Energy* **2013**, *38*, 4901-4934.

[8] P. Lettenmeier, S. Kolb, N. Sata, A. Fallisch, L. Zielke, S. Thiele, A.S. Gago, K.A. Friedrich, *Energy Environ. Sci.* **2017**, *10*, 2521-2533.

[9] Z. Kang, G. Yang, J. Mo, S. Yu, D.A. Cullen, S.T. Retterer, T.J. Toops, M.P. Brady, G. Bender, B.S. Pivovar, J.B. Green Jr., F.Y. Zhang, *Int. J. Hydrogen Energy* **2018**, *43*, 14618-14628.

[10] R. Omrani, B. Shabani, *Int. J. Hydrogen Energy* **2017**, *42*, 28515-28536.

[11] A.T. Pham, T. Baba, T. Shudo, *Int. J. Hydrogen Energy* **2013**, *38*, 9945-9953.

[12] S.A. Grigoriev, P. Millet, S.A. Volobuev, F.N. Fateev, *Int. J. Hydrogen Energy* **2009**, *34*, 4968-4973.

[13] J. Mo, Z. Kang, G. Yang, S.T. Retterer, D.A. Cullen, T.J. Toops, J.B. Green Jr., F.Y. Zhang, *Appl. Energy* **2016**, *177*, 817-822.

[14] S.A. Grigoriev, V.I. Porembsky, V.N. Fateev, *Int. J. Hydrogen Energy* **2006**, *31*, 171-175.

[15] H. Tang, K. Prasad, R. Sanjinès, P.E. Schmid, F. Lévy, *J. Appl. Physics* **1994**, *75*, 2042-2047.

[16] P. Lettenmeier, R. Wang, R. Abouatallah, B. Saruhan, O. Freitag, P. Gazdzicki, T. Morawietz, R. Hiesgen, A.S. Gago, K.A. Friedrich, *Sci. Rep.* **2017**, *7*, 44035.

[17] A. Yilanc, I. Dincer, H. Ozturk, *Progress in Energy and Combustion Sci.* **2009**, *35*, 231-244.

[18] U. Babic, M. Suermann, F.N. Büchi, L. Gubler, T.J. Schmidt, *J. Electrochem. Soc.* **2017**, *164*, F387-F399.

[19] C.M. Hwang, M. Ishida, H. Ito, T. Maeda, A. Nakano, A. Kato, T. Yoshida, *J. Power Sources* **2012**, *202*, 108-113.

[20] P. Lettenmeier, S. Kolb, F. Burggraf, A.S. Gago, K.A. Friedrich, *J. Power Sources* **2016**, *311*, 153-156.

[21] H. Ito, T. Maeda, A. Nakano, A. Kato, T. Yoshida, *Electrochim. Acta* **2013**, *100*, 242 – 248..

[22] C.M. Hwang, M. Ishida, H. Ito, T. Maeda, A. Nakano, Y. Hasegawa, N. Yokoi, A. Kato, T. Yoshida, *Int. J. Hydrogen Energy* **2011**, *36*, 1740-1753.

[23] B. Eladeb, C. Bonnet, E. Favre, F. Lapique, J. Electrochem. Sci. Eng. **2012**, *2*, 211-221.

[24] E. Borgardt, O. Panchenko, F.J. Hackemüller, M. Bram, D. Stolten, W. Lehnert, *J. Power Sources* **2018**, *374*, 84-91.

[25] J.A. Roemer, B.H. McKibben, J.R. Corry, *Method of rolling titanium sheets*, US Patent 2651099, **1953**.

[26] G. Chen, G.Z. Li, C.S. Xiang, S.Y. Zhao, P. Tan, H.P. Tang, P. Cao P, *Powder Metallurgy* **2016**, *59*, 249-255.

[27] G.N. Howatt, R.G. Breckenridge, J.M. Brownlow, *J. Am. Ceram. Soc.* **1947**, *30*, 237-242.

[28] D. Hotza, P. Greil, *Mat. Sci. Eng. A* **1995**, *202*, 206- 217.

[29] M. Jabbari, R. Bulatova, A.I.Y. Tok, C.R.H. Bahl, E. Mitsoulis, J.H. Hattel, *Mat. Sci. Eng. B* **2016**, *212*, 39-61.

[30] M. Bram, R. Kauert, H.P. Buchkremer, D. Stöver, Proc. of Euro-PM 2003, (Ed. EPMA, Shrewsbury, UK) **2003**, *Vol. 2*, 353-359.

[31] Z.S. Rak, J. Walter, *J. Mat. Proc. Techn.* **2006**, *175*, 358-363.

[32] J.E. Bidaux, J. García-Gómez, H. Hamdan, D. Zufferey, M. Rodriguez-Arbaizar, H. Girard, E. Carreño-Morelli, Proc. of Euro-PM 2011, (Ed. EPMA, Shrewsbury, UK) **2011**, *Vol. 2*, 351-355.

[33] Siemens AG, Silyzer 200, Product information, (https://www.siemens.com/global/de/home/produkte/energie/erneuerbare-energien/hydrogen-solutions.html), **2017**.

[34] S. Whitaker, *Transport in Porous Media* **1986**, *1*, 3-25.

[35] K. Bromberger, J. Ghinaiya, T. Lickert, A. Fallisch, T. Smolinka, *Int. J. Hydrogen Energy* **2018**, *43*, 2556-2569.

[36] J.T. Gostick, M.W. Fowler, M.D. Pritzker, M.A. Ioannidis, L.M. Behra, *J. Power Sources* **2006**, *162*, 228-238.

[37] H. Taira, H. Liu, *Int. J. Hydrogen Energy* **2012**, *37*, 13725-13730.

[38] M.S. Ismail, D. Borman, T. Damjanovic, D.B. Ingham, M. Pourkashanian, *Int. J. Hydrogen Energy* **2011**, *36*, 10392-10402.

[39] I.H. Oh, N. Nomura, N. Masahashi, S. Hanada, *Scripta Mat.* **2003**, *49*, 1197-1202.

[40] T. Imwinkelried, *J. Biomed. Mat. Res. A* **2007**, *81*, 964-970.

[41] L.P. Lefebvre, E. Baril, M.N. Bureau, *J. Mat. Sci.: Mater. Med.* **2009**, *20*, 2223-2233.

[42] E. Baril, *Powder Injection Moulding Int.* **2010**, *4*, 22-32.

[43] E.T. Ojong, J.T.H. Kwan, A. Nouri-Khorasani, A. Bonakdarpour, D.P. Wilkinson, T. Smolinka, *Int. J. Hydrogen Energy* **2017**, *42*, 25831-25847.

Figure captions

Figure 1: a.) *Viscosity of slurries comprised of Ti-GA and Ti-HDH powders.* ***b.)*** *Thickness of the green tape after drying as a function of the position of the doctor blade.*

Figure 2: a.) *Green tape in the F500 tape casting device.* ***b.)*** *Microstructure of the green tape produced from Ti-HDH powder.* ***c.)*** *Microstructure of the green tape produced from Ti-GA powder.*

Figure 3: *Thickness profiles of Ti tapes produced from Ti-GA powder* ***a.)*** *on a lab-scale tape casting device and* ***b.)*** *on an automated F500 tape casting device.*

Figure 4: *Microstructures of porous titanium tapes comprised of Ti-GA powders (left-hand side) and Ti-HDH powders (right-hand side), which are dependent on the sintering temperature.* ***a.,b.)*** *Ti-GA-800-250, Ti-HDH-800-250;* ***c.,d.)*** *Ti-GA-900-250, Ti-HDH-900-250;* ***e.,f.)*** *Ti-GA-1000-250, Ti-HDH-1000-250;* ***g.,h.)*** *Ti-GA-1200-250, Ti-HDH-1200-250.*

Figure 5: a.) *Air permeability of porous titanium tapes comprised of Ti-GA powders and Ti-HDH powders as a function of porosity. Measurements were performed under ambient conditions at room temperature.* ***b.)*** *Mean pore radius of porous titanium tapes measured by mercury porosimetry.*

Figure 6: *Tensile strength of the porous titanium tapes as a function of porosity. The thickness of the dog-bone shaped sample was 1mm.*

Figure 7: *Current density–voltage curves of PEM electrolysis cells measured at 80 °C with a titanium-based porous transport layer on the anode side.* ***a.)*** *Ti-GA powder, tape thickness of around 250 µm (Ti-GA-800-250 – Ti-GA-1200-250);* ***b.)*** *Ti-GA powder, tape thickness of around 500 µm (Ti-GA-800-500 – Ti-GA-1200-500);* ***c.)*** *Ti-HDH powder, tape thickness of around 250 µm (Ti-HDH-800-250 – Ti-HDH-1200-250);* ***d.)*** *Ti-HDH powder, tape thickness of around 500 µm (Ti-HDH-800-500 – Ti-HDH-1200-500).*

Figure 8: a.) *Porous transport layer produced by tape casting of Ti-HDH powders. Size in the green state was 470 x 470 mm^2. Sintering was performed at 1000 °C for 2 h in a vacuum.* ***b.)*** *Handling the tapes after sintering.*

Figure 9: *Current density–voltage curve of large PEM cells operated in an industrial electrolyzer. Both configurations were operated in one stack under the same conditions. Comparison of the reference transport layer (blue color) with the novel titanium-based porous transport layer (size 1400 cm²).*

Table of contents

Tape casting titanium powders is a promising method of producing large-scale porous transport layers for polymer electrolyte membrane (PEM) electrolysis cells. It has been proven possible to manufacture tape-cast transport layers of up to 470 x 470 mm^2 in size. The optimum process conditions are defined based on the systematic study of electrochemical and mechanical properties.

Franz Josef Hackemüller, *Elena Borgardt*, *Olha Panchenko*, *Martin Müller*, *Martin Bram**

Manufacturing of large-scale titanium-based porous transport layers for polymer electrolyte membrane electrolysis by tape casting

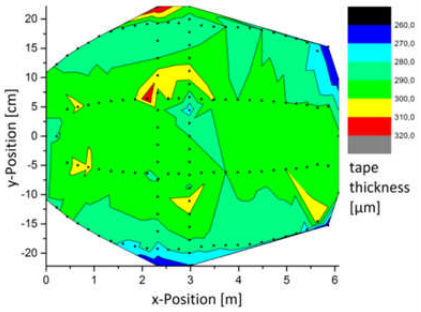

ToC figure

Supplementary Information

Manufacturing of large-scale titanium-based porous transport layers for polymer electrolyte membrane electrolysis by tape casting

*Franz Josef Hackemüller, Elena Borgardt, Olha Panchenko, Martin Müller, Martin Bram**

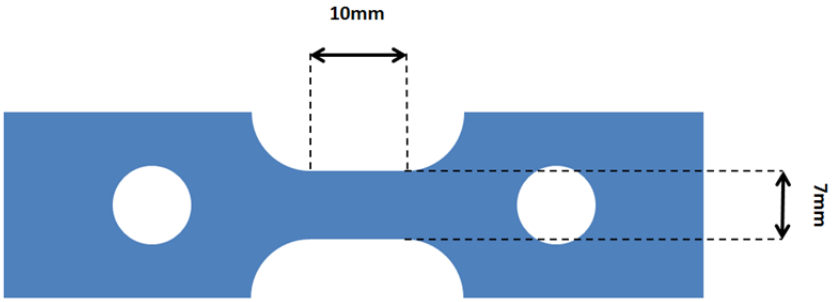

Figure S1. *Schematic of the dog-bone shaped samples for mechanical tests. The thickness of the sample was 1 mm.*

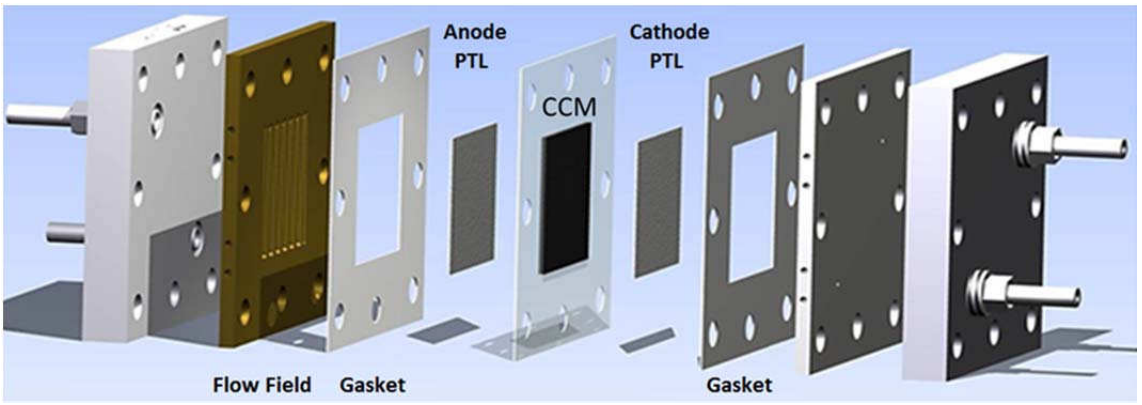

Figure S2. *Exploded-view schematic of the electrochemical testing setup, including porous transport layers (PTLs) and catalyst-coated membrane (CCMs)*